Direct detection of multiple backward volume modes in yttrium iron garnet at micron scale wavelengths

Jinho Lim,[1,*] Wonbae Bang,[1,2] Jonathan Trossman,[1] Andreas Kreisel,[3] Matthias Benjamin Jungfleisch,[2,4] Axel Hoffmann,[2] C. C. Tsai,[5] and John B. Ketterson[1,6,†]

[1]*Department of Physics and Astronomy, Northwestern University, Evanston, Illinois 60208, USA*
[2]*Materials Science Division, Argonne National Laboratory, Argonne, Illinois 60439, USA*
[3]*Institut für Theoretische Physik, Universität Leipzig, D-04103 Leipzig, Germany*
[4]*Department of Physics and Astronomy, University of Delaware, Newark, Delaware 19716, USA*
[5]*Department of Engineering & Management of Advanced Technology, Chang Jung Christian University, Tainan 71101, Taiwan*
[6]*Department of Electrical and Computer Engineering, Northwestern University, Evanston, Illinois 60515, USA*

(Received 6 September 2018; revised manuscript received 3 January 2019; published 28 January 2019)

Using a set of wave-vector-specific multielement antennas, we have characterized the dispersion of spin waves in an yttrium iron garnet film at submicron lengths and resolved the dispersion relations of multiple backward volume modes, particularly in the region of their minima. The techniques developed now facilitate the characterization of spin waves at length scales limited only by available lithography and at a spectral resolution that generally exceeds that of Brillouin scattering. The data obtained are in excellent agreement with theoretical predictions based on a model Hamiltonian.

DOI: 10.1103/PhysRevB.99.014435

I. INTRODUCTION

The dispersion of long-wavelength spin waves in yttrium iron garnet (YIG) has attracted considerable attention over the years [1]. At very long wavelengths the dispersion is governed by magnetostatic effects arising from the requirement that the Maxwell boundary conditions be satisfied at the free surfaces when solving the Landau-Lifshitz equation for the spin precession. A closed form solution for the dispersion in the case of an infinite slab with an in-plane magnetic field was given long ago by Damon and Eshbach [2], and for the case of a perpendicular magnetic field by Damon and Van De Vaart [3]. A full solution for an arbitrarily directed field was given by Bajpai and Srivastava [4].

At shorter wavelengths, the effects of exchange enter, which greatly complicate the analysis. One effect is to push modes that have nodes along the sample thickness to higher frequencies. Kalinikos and Slavin (KS) [5] have obtained an approximate solution for the full angular dependence of the low lying modes in the presence of a model exchange interaction based on perturbation theory. Recently, Arias reported an exact dispersion relation for dipole-exchange spin waves for an arbitrary applied field direction using a Green's function based approach to solve the Landau-Lifshitz equation [6]. A microscopic theory utilizing a model Hamiltonian has been given by Kreisel *et al.* [7] on which we further elaborate below.

Most studies have been limited to the cases where the external magnetic field **H** lies: (i) parallel to the in-plane wave vector **k**, (ii) along the film plane normal **n**, or (iii) in the direction **n** × **k**. The associated modes are designated as backward volume (BV), forward volume (FV), and Damon-Eshbach (DE), respectively; for the first two, the amplitude is distributed throughout the volume of the film, and hence their designation as volume modes, while for the last it is largest at one of the free surfaces and exponentially decays into the interior; the DE mode is also *nonreciprocal* in the sense that the surface on which the mode propagates switches sides when the sign of the field is reversed, making the propagation sensitive to the properties of that surface (e.g., metalized vs not metalized).

The BV mode has the unusual property that, due to the fact that the frequency *decreases* with increasing wave vector at long wavelengths, the group velocity is directed *opposite* to the wave vector, and hence its designation. Inclusion of the exchange interaction causes this downward trend of the mode frequency to go through a minimum at some wave vector, $k_{\min}$, after which it increases approximately as k^2.

Recently two groups have reported that under heavy two-magnon pumping, followed by approximately number-onserving interactions among the excitations so produced and the thermal magnons, a macroscopic *condensation* can result in the two states lying at $k = \pm k_{\min}$, a phenomenon that they refer to as Bose-Einstein condensation [8,9]. Later theoretical work, which accurately reproduces the observed time dependence of the magnon spectrum following pumping, argues that the phenomena should more appropriately be termed a Rayleigh-Jeans condensation [10] since it occurs in the classical portion of the Bose distribution. Regardless of the terminology, this is a clearly an unusual phenomenon and hence it is important to have a more complete characterization of the magnon spectrum in the vicinity of where it occurs.

Here we report measurements of short wavelength (micron and submicron scale) spin waves in an yttrium iron garnet film. Historically, the preferred tool to study spin waves in this regime has been Brillouin scattering (BLS) from the thermally

*JinhoLim15.2014@u.northwestern.edu
†j-ketterson@northwestern.edu

excited modes [11]. With this technique the wave vector is fixed by the scattering angle; however (apart from any intrinsic lifetimes), the resolution is typically limited by spectral broadening of the incident laser together with the resolution of the spectrometer that analyzes the inelastically scattered light, which is generally a multipass Fabry-Perot cavity [12]. These instrumental factors typically limit the precision of frequency determinations to a few percent. As we demonstrate below, in the present investigation there are multiple, close-lying modes, which cannot be resolved with the BLS technique. For example, a typical frequency resolution of BLS is 250 MHz [8], but the smallest frequency spacing between these modes in our study is 65 MHz. Furthermore, the linewidths associated with the resonances reported here are in the range 10–20 MHz, less than 10% of that characteristic of BLS.

The frequencies of long-wavelength spin waves studied typically lie in the microwave regime. However, their wavelengths differ from those of the corresponding electromagnetic waves by factors of order 10^5, so coupling to spin waves presents a challenge. Millimeter spin waves in YIG films are readily studied by launching and receiving the waves from opposing edges of a sample with adjacent wire antennas [13] (or pairs of metallic stripes patterned directly on the film surface). However, this approach becomes increasingly problematic at wavelengths below about approximately 100 microns due to rough or nonparallel edges (or finite width of the patterned stripes).

Here we present an alternate technique, which was earlier suggested on theoretical grounds [14,15], in which a multielement antenna consisting of an array of parallel stripes is patterned on the film so as to directly couple to various modes having a wavelength λ matching the stripe spacing d of the antenna elements (or a submultiple thereof). The only spectral limitation (again apart from the intrinsic lifetime) is set by the number of elements n in the antenna, which determines the precision with which the wavelength is resolved according to $\Delta\lambda \approx \lambda/n$ where n is the number of elements. An inconvenience of this approach is that multiple antennas must be patterned, one for each wavelength (together with its subharmonics). Yu *et al.* [16] and Liu *et al.* [17] have used similar technique to generate spin waves. We recently performed measurements on a YIG film with a multielement antenna having a 50-μm spacing [18] where we studied the angular dependence of modes having this wavelength as well as the odd spatial subharmonics of 16.6 and 10 μm. To cover the range of interest in the present work four different antennas were patterned with spacings of 0.6, 1, 3, and 10 μm; details on the patterning of these antennas are described below.

The dynamic magnetic fields produced by the antenna are essentially magnetostatic in character and the associated scalar potential must therefore satisfy Poission's equation. Approximating the potential so produced by a strictly periodic form of infinite extent involves the form

$$\phi(x,z,t) = \Re e^{-i\omega t} \sum_n \phi_{0n} \cos(k_n x) e^{-k_n z}; \qquad (1)$$

here $k_n = 2\pi n/d$ where d is the rung spacing and the associated microwave field $\mathbf{H}_\mu$ follows from $\mathbf{H}_\mu = \nabla\phi$. Therefore,

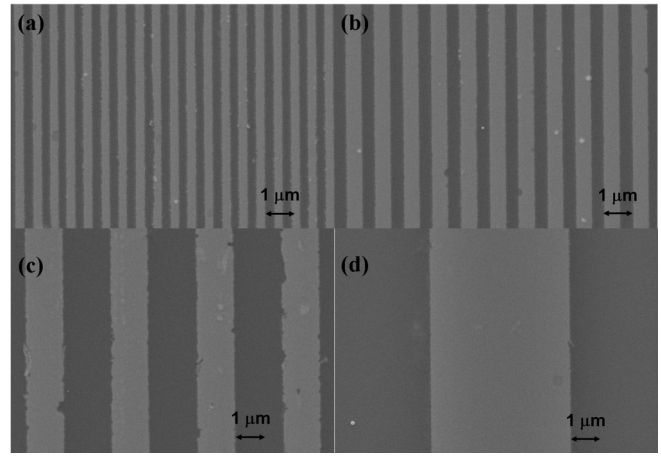

FIG. 1. SEM images at the same magnification of the multielement antennas on a YIG film with periods of (a) 0.6 μm, (b) 1 μm, (c) 3 μm, and (d) 10 μm.

the behavior of the magnetic field along the film thickness direction involves the *same characteristic lengths* that govern the spacing between the antenna rungs, which fix the wavelength of any spin waves generated. This property allows coupling to the higher-frequency exchange split modes associated with quantization along the film thickness direction. In particular this property facilitates coupling to the higher-lying backward volume mode in the vicinity of $k_{\min}$.

II. SAMPLE PREPARATION

The yttrium iron garnet (YIG) film used in these experiments was grown by liquid phase epitaxy on a lattice matched (111) gadolinium gallium garnet (GGG) substrate (5 mm × 10 mm) and was supplied by MTI Corp [19]. The film thickness was determined as 2.843 ± 0.002 μm using an M-2000 ellipsometer (J. A. Woollam Co.), which is comparable to the periods of the antennas utilized.

Our multielement antennas have a ladder geometry and consist of two contact pads connected by 100 rungs, each 500 μm long; they were fabricated directly on the YIG film surface. The contact pads (700 μm^2) consist of 5 nm of Ti followed by 100 nm of Au which were deposited by electron-beam evaporation and patterned by optical lithography using a laser writer; here the Ti layer enhances the adhesion of the Au layer to the YIG film. A bilayer lift-off process was utilized to pattern the antenna rungs using electron-beam lithography followed by electron-beam evaporation of Ti and Au with the same thicknesses as used for the pads. The base pressure during the film deposition was $\sim 3.0\times10^{-7}$ Torr, and the film thicknesses were monitored by a quartz crystal microbalance.

Figure 1 shows four scanning electron microscope (SEM) images, each at the same magnification, of the active region of the multielement antennas on the YIG film which have periods of 0.6, 1, 3, and 10 μm. The ratio between the width of the rung and spacing was 1:1. The lighter parts in Fig. 1 correspond to the Au antenna elements, while the darker parts correspond to the underlying YIG film.

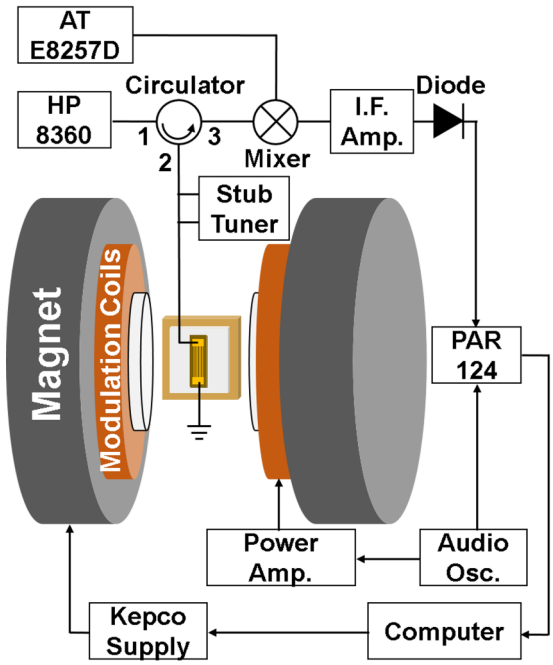

FIG. 2. A schematic of the FMR measurement system. A 200-μm-thick glass cover slip creates a gap between the YIG film and the Cu base plate of the sample holder to avoid any effects from an adjacent conducting surface.

III. EXPERIMENTAL TECHNIQUES

Figure 2 shows a schematic of the measurement setup. To enhance the signal relative to the background, the field modulation technique was used with associated frequencies nominally in the range 10–1000 Hz. Microwave signals in the range of 1–8 GHz and power levels of 20–25 dBm from a signal generator (Hewlett Packard 8360) were passed from port 1 to port 2 of a three-port circulator (Pasternack PE8402) and transmitted into a multielement antenna. A stub tuner (Maury Microwave 1719B) is placed between the sample and port 2, which is used to balance the resulting microwave bridge. The reflected signal from the antenna again passed through the circulator (from port 2 to port 3), from which it went to a microwave mixer. The output of a second microwave generator (Agilent AT E8257D) served as a local oscillator and the resulting mixed 10-MHz signal was fed to an i.f. amplifier (Anzac AM-112) the output of which was rectified by a microwave diode and sent to a lock-in amplifier (PAR 124) operating at the modulation frequency. The whole apparatus is controlled by a computer operating under LabVIEW which generates a ramp to sweep the magnet and records the outputs of the lock-in and a Hall probe; signal averaging is utilized to detect the relatively weak absorption from the antennas at the spin-wave resonances.

Figure 3 shows some typical signal averaged data at 7.4 GHz generated from an antenna with a 10-μm period; data at other wavelengths show a similar behavior. Typical linewidths are approximately 3–6 G corresponding to a frequency of 9–18 MHz. Since these data were obtained from a field sweep, resonances observed at fields above the uniform ferromagnetic resonance (FMR) field would correspond to frequencies below the uniform FMR frequency in a frequency sweep. Since our antenna has 1:1 ratio of the electrode width to electrode spacing, all even Fourier harmonics are suppressed; therefore, the first spatial harmonic will be for $n = 3$, and the corresponding wavelength will be 10 μm$/n = 3.3$ μm. Also, there is an amplitude variation among the three low-lying 10-μm BV resonances since these modes have different behaviors, arising from the boundaries and nodes along film thickness direction, whereas they have the same in-plane wavelength (10 μm). From Eq. (1), the

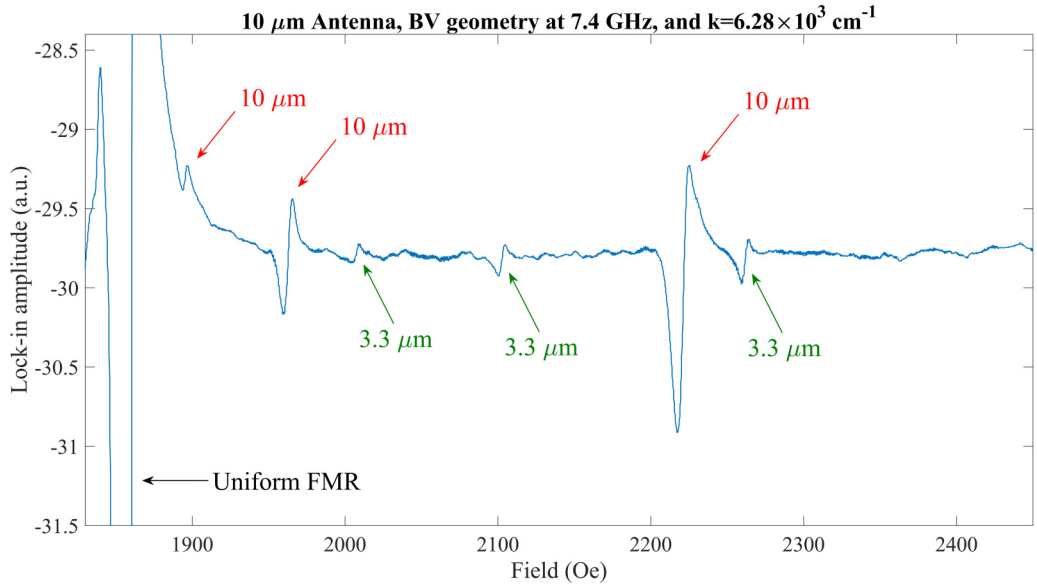

FIG. 3. An example of raw data generated from a 10-μm period antenna. There are three classes of signals. The first, which is off scale, arises from the uniform precession mode (FMR), the second is caused by the three lowest-lying BV modes having an in-plane wavelength of 10 μm, and the last is from the corresponding three BV spin waves with an in-plane wavelength of 3.3 μm generated from the first odd spatial subharmonic ($n = 3$) of the antenna.

time-varying magnetic field generated by the 10-μm antenna has an amplitude which decays exponentially along the film thickness direction with a characteristic length of 10 μm. Since the next highest frequency mode in the presence of the exchange interaction has a wavelength of $s/2$ ($\approx$1.4 μm), where s is the thickness of the YIG film, its amplitude is suppressed relative to the lowest-lying mode.

IV. THEORETICAL MODELING

In order to theoretically obtain the expected eigenfrequencies of our thin-film ferromagnet, we use a microscopic approach that is based on a model of localized spins on a cubic lattice. These spins are coupled by nearest-neighbor exchange interactions and, in addition, are subject to long-range dipole-dipole interactions. Such a microscopic model has been solved previously for thin films of YIG using a numerical method [7]. The necessary steps are (i) determining the spin structure in the classical limit, (ii) mapping it to bosonic degrees of freedom, and (iii) diagonalizing the resulting Hamiltonian. For a ferromagnetic film with an in-plane field, the classical energy is minimized if the magnetization points in the direction of the field. The mapping is done using the Holstein-Primakoff transformation. Because the effective spin $S \approx 14.2$ in YIG is very large [5], it is sufficient to restrict to the leading term of the $1/S$ expansion (linear spin-wave theory). The resulting model is that of noninteracting bosons on a cubic lattice, which can be considered as infinite for the in-plane directions and finite across the thickness of the film. Thus, a two-dimensional Fourier transformation yields a Hamiltonian that is diagonal in the in-plane momentum quantum numbers and consists in a $2N \times 2N$ matrix where N is the number of lattice points across the thickness d, i.e., such that $Na = d$ where a is the lattice constant. The remaining steps are (a) numerical diagonalization of the Hamiltonian by means of an antiunitary transformation [20] to obtain the eigenenergies (modes) for each fixed in-plane momentum, and (b) setting up the Hamiltonian by calculating the (partial) Fourier transform of the original interaction terms [7,21]. For the nearest-neighbor exchange couplings, this can be done straightforwardly, while for the dipolar long-range interactions, we use Ewald summation techniques to obtain the coefficients with high precision [7].

V. COMPARISON OF THEORY AND EXPERIMENT

We observed that the uniform precession frequency of the patterned YIG film was somewhat shifted from that for an isolated YIG film. This is likely due to the presence of the metallic electrodes, since they are patterned directly on the surface of the sample. In particular, the patterning may alter (i) the electromagnetic boundary conditions (due to the presence of the metals) and/or (ii) the surface spin pinning conditions. If such effects indeed arise from the metal electrodes a realistic inclusion of the resulting effect(s) is beyond the scope of the present investigation. To phenomenologically account for such effects we used two different models. First, we used a modified saturation magnetization, $4\pi M_s = 1.94 \times 10^3$ emu/cm^3, which is equivalent to introducing a uniaxial anisotropy energy into the in-plane Kittel

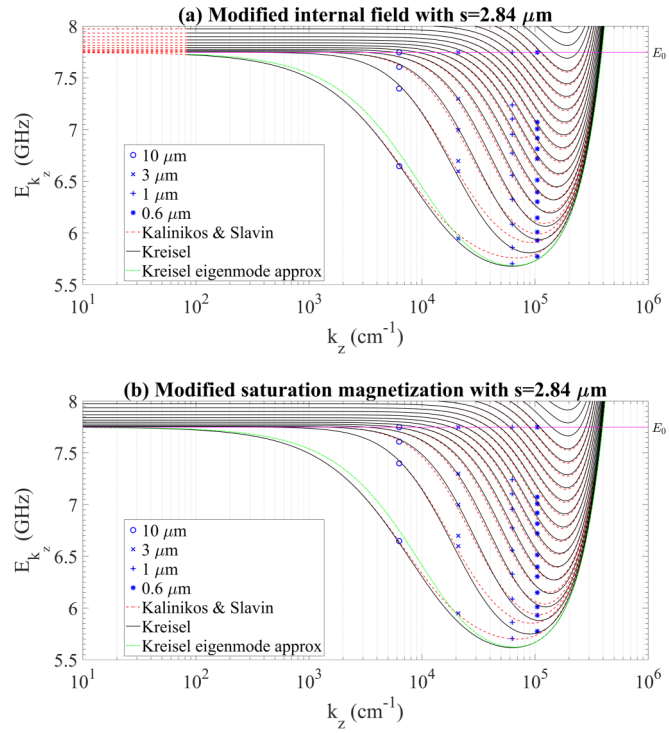

FIG. 4. The measured frequencies of the lowest-lying, and the first few exchange split, backward volume spin waves in a 2.84-μm-thick YIG film at wavelengths of 10, 3, 1, and 0.6 μm. Shown also are the microscopic calculations involving the model spin Hamiltonian (black solid line) together with an approximate treatment based on a Fourier expansion of the magnetostatic Landau-Lifshitz equation (red dashed line). (a) shows the comparison using a modified internal field while (b) shows that for a modified saturation magnetization. Also shown is an approximate treatment due to Kreisel *et al.* [7] (green dot-dashed line). Finally, the points on the line designated E_0 correspond to the $k = 0$ (uniform) FMR mode.

formula, $\omega = \gamma\sqrt{H(H + 4\pi M + 2K)}$ (Kalinikos *et al.* [22]). Second, we used a modified internal field, $H_{\rm mod} = H + 28.28$ Oe. Both of these shifts were obtained by fitting the position of the uniform FMR mode.

Our raw data consist of files of the lock-in output amplitude vs magnetic field at four different frequencies. To generate frequency vs wave-vector plots, we interpolated the data from experiments at the four frequencies to obtain the frequencies at the field value that was used in the theoretical modeling for each of the four different wavelengths patterned. In this way we can compare experiment and theory in the form of the frequency vs wave-vector dispersion relation.

Figures 4(a) and 4(b) summarize the observed spin-wave resonances at the four wavelengths studied together with the numerical results (black solid lines) arising from the model Hamiltonian described above and our two fitting approaches to account for the FMR frequency shift. Also shown are the results (red dashed lines) from the Kalinikos-Slavin (KS), approximation based on a Fourier expansion of the magnetostatic Landau-Lifshitz equation with an unpinned boundary condition on both surfaces [5] and the same fitting parameters. Note that for the lowest eigenmode, there are schemes for analytically calculating the eigenfrequencies based on an ansatz

for the amplitudes of the spin waves across the film [5,23], or the solution of the mangetostatic boundary value problem [24]. The green dot-dashed line in Fig. 4 was given earlier by Kreisel *et al.* [7]. Note that the position of the minimum of the lowest mode is better reproduced in the Kreisel model when we use a modified internal field whereas the KS model agrees better when we use a modified saturation magnetization.

VI. CONCLUSIONS

In conclusion we have carried out measurements of the dispersion of the low-lying backward volume spin-wave modes in YIG in a regime where dipolar and exchange effects compete on an equal footing. Not only is the lowest-lying branch characterized but, depending on the wavelength, between four and 12 of the higher-lying branches are resolved. This is made possible through the high resolution achieved: a few parts in a thousand, which rivals that achievable with Brillouin scattering. The data are in excellent agreement with microscopic calculations based on a model Hamiltonian for YIG. Especially interesting will be experiments under high amplitudes of excitation where the unusual condensation phenomenon discussed above has been reported [8,9]. Quite generally, the techniques developed open the way to perform various experiments involving spin wavelengths in the micron range. In particular, our approach is applicable to metallic systems provided a suitable insulating layer is incorporated to electrically isolate the antenna. Using more advanced lithographic techniques, still shorter wavelengths should be accessible.

ACKNOWLEDGMENTS

The magnetic resonance measurements were performed at Northwestern University under support from the U.S. Department of Energy through Grant No. DE-SC0014424. Device fabrication was carried out at Argonne and supported by the U.S. Department of Energy, Office of Science, Materials Science and Engineering Division. Lithography was carried out at the Center for Nanoscale Materials, an Office of Science user facility, which is supported by DOE, Office of Science, Basic Energy Science under Contract No. DE-AC02-06CH11357.

[1] For a review see, A. A. Serga, A. V. Chumak, and B. Hillebrands, J. Phys. D: Appl. Phys. **43**, 264002 (2010).
[2] R. W. Damon and J. R. Eshbach, J. Phys. Chem. Solids **19**, 308 (1961).
[3] R. W. Damon and H. Van De Vaart, J. Appl. Phys. **36**, 3453 (1965).
[4] S. N. Bajpai and N. C. Srivastava, Phys. Status Solidi A **57**, 307 (1980).
[5] B. A. Kalinikos and A. N. Slavin, J. Phys. C: Solid State Phys. **19**, 7013 (1986).
[6] R. E. Arias, Phys. Rev. B **94**, 134408 (2016).
[7] A. Kreisel, F. Sauli, L. Bartosch, and P. Kopietz, Eur. Phys. J. B **71**, 59 (2009).
[8] S. O. Demokritov, V. E. Demidov, O. Dzyapko, G. A. Melkov, A. A. Serga, B. Hillebrands, and A. N. Slavin, Nature (London) **443**, 430 (2006).
[9] O. Dzyapko, V. E. Demidov, G. A. Melkov, and S. O. Demokritov, Philos. Trans. R. Soc. A **369**, 3575 (2011).
[10] A. Ruckriegel and P. Kopietz, Phys. Rev. Lett. **115**, 157203 (2015).
[11] S. O. Demokritov, B. Hillebrands, and A. N. Slavin, Phys. Rep. **348**, 441 (2001).
[12] J. R. Sandercock, in *Light Scattering in Solids III*, edited by M. Cardona and G. Güntherodt (Springer, Berlin, 1982).
[13] J. Lim, J. Trossman, C. C. Tsai, W. Bang, and J. B. Ketterson, J. Magn. Magn. Mater. **456**, 241 (2018).
[14] B. A. Kalinikos, IEE Proc. Part H: Microwaves, Opt. Antennas **127**, 4 (1980).
[15] S. A. Bogacz and J. B. Ketterson, J. Appl. Phys. **58**, 1935 (1985).
[16] H. M. Yu, O. D. Kelly, V. Cros, R. Bernard, P. Bortolotti, A. Anane, F. Brandl, F. Heimbach, and D. Grundler, Nat. Commun. **7**, 11255 (2016).
[17] C. P. Liu, J. L. Chen, T. Liu, F. Heimbach, H. M. Yu, Y. Xiao, J. F. Hu, M. C. Liu, H. C. Chang, T. Stueckler, S. Tu, Y. G. Zhang, Y. Zhang, P. Gao, Z. M. Liao, D. P. Yu, K. Xia, N. Lei, W. S. Zhao, and M. Z. Wu, Nat. Commun. **9**, 738 (2018).
[18] J. Lim, W. Bang, J. Trossman, D. Amanov, C. C. Tsai, M. B. Jungfleisch, A. Hoffmann, and J. B. Ketterson (unpublished).
[19] MTI Corporation, 860 S. 19th Street, Richmond, CA, USA.
[20] A. A. Serga, C. W. Sandweg, V. I. Vasyuchka, M. B. Jungfleisch, B. Hillebrands, A. Kreisel, P. Kopietz, and M. P. Kostylev, Phys. Rev. B **86**, 134403 (2012).
[21] R. N. Costa Filho, M. G. Cottam, and G. A. Farias, Phys. Rev. B **62**, 6545 (2000).
[22] B. A. Kalinikos, M. P. Kostylev, N. V. Kozhus, and A. N. Slavin, J. Phys.: Condens. Matter **2**, 9861 (1990).
[23] S. M. Rezende, Phys. Rev. B **79**, 174411 (2009).
[24] G. Li, C. Sun, T. Nattermann, and V. L. Pokrovsky, Phys. Rev. B **98**, 014436 (2018).